Macromolecules
ARTICLE

Macromolecules **2010**, *43*, 7269–7276 **7269**
DOI: 10.1021/ma101113g

Effect of Grafting Density on Phase Transition Behavior for Poly(*N*-isopropylacryamide) Brushes in Aqueous Solutions Studied by AFM and QCM-D

Naoyuki Ishida[†,‡] **and Simon Biggs***[,†]

[†]*School of Process, Environmental and Materials Engineering, University of Leeds, Leeds LS2 9JT, U.K., and* [‡]*Photonics Research Institute, National Institute of Advanced Industrial Science and Technology (AIST), 1-1-1 Higashi, Tsukuba 306-8565, Japan*

Received May 19, 2010; Revised Manuscript Received July 25, 2010

ABSTRACT: The effect of grafting density on the phase transition behavior of poly(*N*-isopropylacrylamide) (PNIPAM) grafted onto a flat substrate was investigated using an atomic force microscope (AFM) and a quartz crystal microbalance (QCM-D). We prepared PNIPAM brush layers at three different grafting densities on silicon wafers using a "grafting from" atom transfer radical polymerization (ATRP) approach. AFM imaging in water at various temperatures showed that the transition behavior of the grafted PNIPAM chains from a brush-like to a mushroom-like morphology was dependent on the grafting density: the images change abruptly from essentially featureless to domain structures across the LCST for the low-density surface, whereas the change in the images becomes less abrupt with increasing polymer graft density. The QCM-D data also indicated a significant dependence of the layer properties on the grafting density, confirming the behavior differences suggested by the AFM images. In particular, the dissipation data strongly suggest that the magnitude of lateral aggregation for the PNIPAM chains depends on the grafting density. A similar effect of grafting density was also observed for the phase transition as a function of salt concentration in sodium sulfate solutions.

Introduction

Poly(*N*-isopropylacrylamide) (PNIPAM) is the most popular and well-investigated temperature-responsive polymer; this is largely due to it having a lower critical solution temperature (LCST) at around 32 °C.[1] PNIPAM chains hydrate to swell and stretch in aqueous solutions at temperatures below the LCST, while they shrink to take a globular form at temperatures higher than the LCST with a sharp phase transition in bulk solution across the LCST due to dehydration. This feature gives PNIPAM great potential for applications in a wide range of fields such as engineering, biotechnology, and medicine. By grafting PNIPAM chains onto a solid surface, one can potentially utilize this hydration/dehydration effect across the LCST since the collapse of the PNIPAM can drive a hydrophilic/hydrophobic transition in addition to structural deformations of the grafted layers. Thus, such PNIPAM or PNIPAM-based copolymers grafted onto surfaces are expected to have a very wide range of useful applications, including liquid chromatography,[2−4] permeation-controlled filters,[5,6] chemical sensors,[7−9] cell culture,[10,11] attachment−detachment controllable surfaces for proteins[12,13] and living cells,[14,15] medical diagnostic devices,[16,17] and functional composite surfaces.[18]

If such surface-grafted PNIPAM layers are to be used in this wide variety of applications, it is important to understand the detailed behavior of the grafted PNIPAM chains under different conditions. Optimization of the conformational changes in these layers for specific functions is clearly an important goal. The behavior of grafted PNIPAM onto surfaces has been extensively studied using a range of techniques including dynamic light scattering (DLS),[19−21] surface plasmon resonance (SPR),[22] neutron reflectivity (NR),[23−27] quartz crystal microbalance measurements (QCM),[28−31] atomic force microscopy (AFM),[32−34] and surface forces.[35−37] Among the factors that influence structural changes of grafted PNIPAM, both the grafting density and the molecular weight of the PNIPAM brushes have been shown to have a critical importance.[22−27,35−37] Balamurugan et al.[22] found, using SPR, that the collapse transition for a high-density PNIPAM brush, prepared by atom transfer radical polymerization (ATRP), occurs over a relatively broad range of temperatures across the LCST. This observation is considerably different than the sharp structural change, which is often predicted in the case of high molecular weight (long) polymer chains with a low grafting density, reported in a number of previous works.[19,20] Yim et al. have also reported in a series of papers using NR that the magnitude of chain conformational changes alters in a complicated way depending on the combination of the grafting density and the molecular weight of the polymer.[23−26] Some more recent studies report that grafted PNIPAM chains with very low molecular weights do not collapse, even at temperatures well above the LCST.[35,36] Efforts have also been taken to describe theoretically such phase behavior for end-grafted polymers using several models,[38−40] and these reports have predicted that the phase behavior of grafted brushes should depend on both the molecular weight and grafting density of the chains, as is seen empirically.

While most of these earlier studies have focused on changes in the grafted layer perpendicular to the grafted surface, such as the thickness of the layer and its first moment density profile for the chains, the morphological changes, and associated spatial variations parallel to the surface, for the grafted PNIPAM across the LCST have not been well characterized, to date. Hence, direct visual information about the influence of grafting density and/or the molecular weight on the morphological behavior of end-grafted PNIPAM layers should provide important insight.

*To whom correspondence should be addressed. E-mail: s.r.biggs@leeds.ac.uk.

Published on Web 08/06/2010

In previous studies,[41,42] we reported *in situ* AFM images showing a considerable structural change in a PNIPAM layer with relatively low grafting density (0.0088 chains/nm^2) and high molecular weight (655 kDa), prepared by radical graft polymerization using AFM in water and salt solutions. In these works, we successfully observed a sharp conformational change of the PNIPAM layer due to the phase transition from a brush to mushroom state at the LCST in water and at the particular concentration in sodium sulfate solutions. We also demonstrated that quartz crystal microbalance with dissipation monitoring (QCM-D) measurements had excellent versatility as a tool to investigate grafted polymers on solid surfaces especially when combined with direct visual evidence of the state of the layers from AFM images. Under the conditions of the experiments reported, a sharp transition of the polymer layer at the LCST was clearly detected as large signal changes of both frequency and dissipation.

In the present study, we focus mainly on the effect of polymer grafting density on morphological changes of end-grafted PNIPAM. We have prepared the PNIPAM layers with varied grafting densities by ATRP to ensure the molecular weight for each sample is essentially constant. These surfaces were analyzed by visualizing the morphological change of the surface through the phase transition using AFM and by detecting these structural changes using QCM-D both in water at various temperatures and in salt solutions at various concentrations and at a fixed (room) temperature.

Experimental Section

Materials. Silicon wafers (Nilaco, Japan) were used as test surfaces, and they were cut in ca. 1.5 × 1.5 cm pieces. Polished, AT-cut quartz crystal QCM sensors (1.4 cm in diameter) with a coating of a thin silicon oxide layer (Q-Sense AB, Sweden) were used for QCM measurements. *N*-Isopropylacrylamide (NIPAM) was obtained from Aldrich and recrystallized from hexane. Dicyclohexyldicarbodiimide (DCC), *p*-(dimethylamino)pyridine (DMAP), ethyl 2-bromoisobutryate (EBiB), dichloromethane, 3-aminopropyltriethoxysilane (APS), 3-metacryoxypropyltriethoxysilane (MPS), Cu(I)Br, and 2,2′-bipyridine (all from Aldrich) were used without further purification. All water used in experiments was Millipore Milli-Q grade.

Grafting of PNIPAM on Surfaces. PNIPAM-grafted surfaces were prepared on the silicon wafers and the QCM sensors by ATRP. Scheme 1 outlines the procedure for the preparation of PNIPAM polymer brushes. Prior to grafting, the silicon wafers were cleaned in a 7:3 mixture of concentrated sulfuric acid and hydrogen peroxide (piranha solution) at 70−80 °C for 30 min to remove contamination and ensure the formation of an oxide layer on the surface. *Caution*: *piranha solution is a hazardous oxidizing agent and can react violently with organics*. After rinsing with pure water, they were sonicated in a 5 mM sodium hydroxide solution for 5 min and rinsed again with pure water. The QCM sensors were cleaned by UV irradiation (∼9 mW cm^{-2} at 254 nm) for at least 15 min, followed by sonication in a 5 mM sodium hydroxide solution and then a thorough rinsing with water.

The cleaned wafers and the QCM sensors were silanated by the immersion into mixed solutions of APS and MPS in 95/5 vol % ethanol/water for 1 h, washed twice with ethanol, and dried. After the silanation, the following treatment[43] was conducted to form Br-bearing group which acts as ATRP initiator on the surfaces. The silanated wafers and sensors were immersed into a solution of 0.20 mmol of 2-bromo-2-methylpropionic acid and 0.05 mmol of DMAP in 10 mL of dichloromethane, and the solution was cooled to 0 °C. Then 0.25 mmol of DCC was added, and the solution was left overnight at room temperature. After the reaction, the surfaces were rinsed with dichlorometane and acetone and dried with a nitrogen stream. In this process, varying the ratio of APS and MPS can alter the grafting density of the polymer because only amino group of APS is transferred to Br-bearing group.

Scheme 1

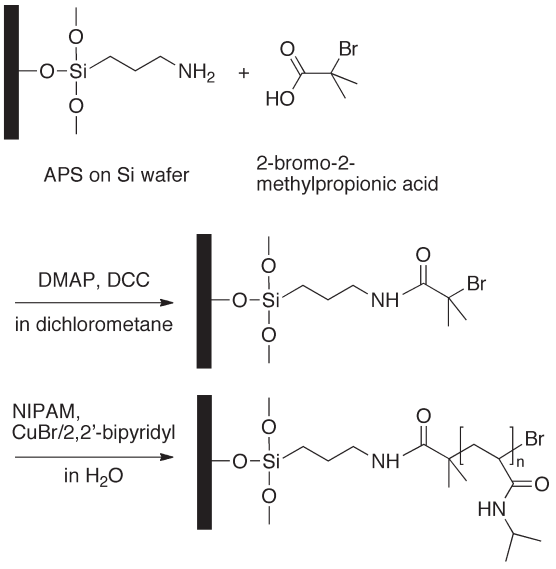

Regents for generating Br-bearing group

2-bromo-2-methylpropionic acid	DMAP	DCC	dichlorometane
33.4mg (0.20 mmol)	6mg (0.05 mmol)	51.3mg (0.25 mmol)	10mL

Table 1. Characteristics of Grafted PNIPAM Brushes

substrate	sample	grafting density (molecule/nm^2)	molecular weight (g/mol)	polydispersity index
silicon wafer	HD	0.361	216 000	1.28
	MD	0.071		
	LD	0.018		
QCM sensor	HD	0.337	197 000	1.21
	MD	0.042		
	LD	0.015		

For polymer grafting, a solution of NIPAM (17.7 mmol), CuBr (0.177 mmol), and 2,2′-bipyridyl (0.354 mmol) in 20 mL of water was deoxygenated by the bubbling of nitrogen gas. This solution was then transferred to a glass bottle which contains the Br-modified silicon wafers and QCM sensors under a nitrogen environment. The polymerization was allowed to proceed at room temperature. A part of the solution was separated, and ethyl 2-bromoisobutyrate was added in the separated solution to produce free polymer. After the reaction, the surfaces were immersed in cold water overnight to remove any unbound reagents and then rinsed extensively with water and dried with a nitrogen stream. The free polymer formed in the separated solution was precipitated in cold methanol and collected to measure the molecular weight.

The grafting density of the PNIPAM layer was estimated by measuring dry thickness and molecular weight of the grafted layer. The thickness of the layer was measured with Stokes ellipsometer (LSE, Gaetner Scientific). The molecular weight of the grafted PNIPAM was estimated by measuring the molecular weight of the free PNIPAM, under the assumption that the grafted and the free PNIPAM have the same molecular weight. The measurement of the molecular weight of the free PNIPAM was conducted with gel permeation chromatography (Waters, Japan) analysis with polystyrene standards for calibration. DMF with 0.01 M LiBr (flow rate: 1 mL/min) was used as mobile phase.

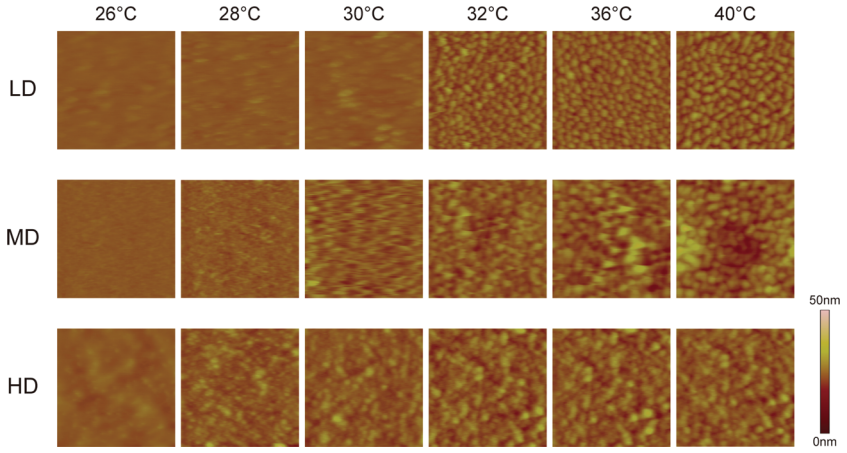

Figure 1. AFM images ($1 \times 1\ \mu m^2$) of a PNIPAM layer on silicon wafer in water for the LD, MD, and HD surfaces. Images were obtained at 26, 28, 30, 32, 36, and 40 °C.

We prepared three PNIPAM-grafted surfaces with different grafting densities, which we term high, middle, and low densities (hereafter HD, MD, and LD surfaces, respectively). The characteristics of the samples are given in Table 1. For the graft polymerization onto both the silicon wafers and the QCM sensors, all the samples were treated in the same batch. Thus, we assumed that the three samples have the same molecular weight and polydispersity for the grafted chains as shown in the table.

AFM Measurements. *In situ* imaging of the grafted PNIPAM in solutions was performed with a Nanoscope IV atomic force microscope (Veeco). Images were collected using the soft-contact method.[44] All images presented are height images and have been zero-order flattened using a standard algorithm within the Nanoscope software to remove artificial height offsets between consecutive scan lines of the raw images. Triangular cantilevers with an integral silicon nitride tip (OMCL-TR, Olympus, Japan) with nominal spring constant 0.15 N/m were used for all AFM experiments and were cleaned using UV irradiation prior to use. The solutions used were passed through 0.2 μm filter (GHP Acrodisc, Pall Gelman Science) mounted on a syringe as they were injected into the AFM fluid cell. Imaging was started after 2 h from the injection of solution to the liquid cell for the hydration of the grafted chains on the surfaces. The solution temperature was varied and kept constant using the temperature-controlling system for Nanoscope (Veeco). The system consisted of a heat stage mounted on top of the scanner and a controller which adjusts temperature of the stage by providing electric current. The solution temperature was monitored with a small thermocouple inserted into the liquid cell. The deviation of temperature was estimated to be within 0.1 °C.

QCM-D Measurements. A commercial QCM-D (Q-300, Q-Sense AB, Sweden) was used to perform all the QCM-D measurements. In a typical QCM experiment, the shift in resonant frequency (Δf) of a piezoelectric quartz crystal is directly monitored and this shift in frequency is often related to the mass on the surface (Δm) according to the Sauerbrey equation:[45]

$$\Delta m = -C\frac{\Delta f}{n}$$

where m is the adsorbed mass, C is a constant characteristic of the crystal, and n is the overtone number (1, 3, 5, ...).

In addition to mass measurements, the dissipation monitoring enables one to evaluate the relative viscoelastic properties of layers on the surface. The measurement of the dissipation (ΔD) is performed by turning the driving voltage off periodically and monitoring the decay of the oscillation after turning off the voltage. When a layer on the surface is rigid, the decay of the oscillation is relatively slow, while for a viscoelastic layer the decay is fast due to the dampening effect of the layer.

The QCM-D data presented here are those measured at the third overtone (~15 MHz). This overtone has better signal-to-noise and is less affected by the cell mounting than other overtones.[46] The solution in the chamber was maintained at desired temperature with the deviation within 0.02 °C. For every temperature of the measurement, the values of Δf and ΔD were allowed to equilibrate, for typically at least 45 min.

Results and Discussion

In Water at Various Temperatures. *In situ* AFM images of the PNIPAM-grafted surface obtained for the three different grafting densities at various temperatures are shown in Figure 1. Around room temperature (26 °C), the images for all the surfaces were essentially featureless, and only very subtle indications of any structural features were seen. The LD surface still showed no strong evidence for significant structure in the images until temperature was increased up to 30 °C, even though somewhat subtle features can be seen with increasing temperature. When the temperature was increased close to the LCST, 32 °C, a large number of domain-like structures were seen to appear on the image, and these structures remained as the temperature was further increased. These images indicate clearly that the PNIPAM layer undergoes an abrupt structural change from a brush-like to a mushroom-like state across the LCST. These domain-like structures were seen to provide sharper contrast within the images as the temperature increased further after the phase transition, suggesting that these structures become progressively more rigid. These data are consistent with those reported previously, by us, for surface-grafted PNIPAM prepared using free-radical graft polymerization. Our previous data were collected using a system that has a higher molecular weight and a lower graft density than the current LD surface.[41]

When the grafting density is increased, the structural transition as a function of the temperature alters, as is seen in Figure 1. The image of the MD surface initially showed some apparent structural features at around 28 °C. The contrast of these structures in the images becomes sharper at 30 °C and then shows a stable domain-like shape at around 32 °C. This possibly indicates the start of a phase transition at a lower temperature than was seen for the LD surface; the transition also seems to occur over a broader range of temperature than for the LD surface. For the HD surface, the AFM images suggest that the phase transition happens over an even broader range of temperature than was seen for the MD case. The image at 28 °C already shows domain structures even though the temperature is well below the bulk solution LCST. Increasing the temperature also increased the

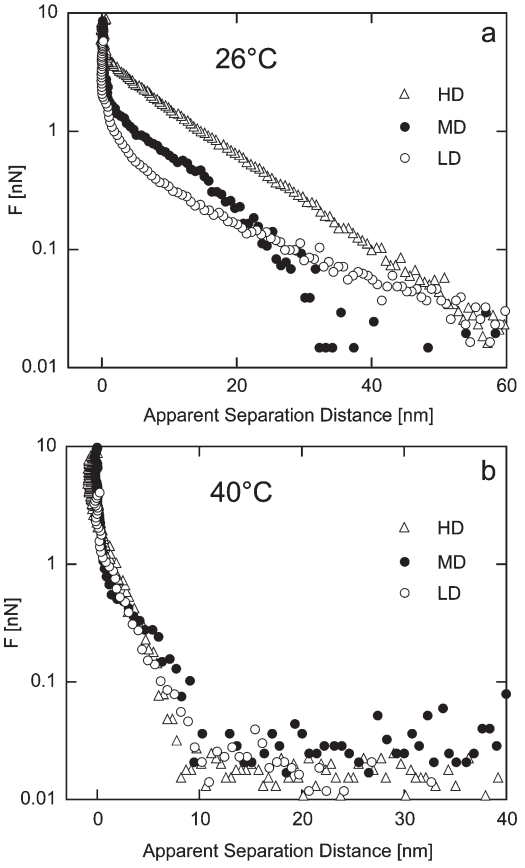

Figure 2. Semilog plot of the interaction forces between the PNIPAM layer and probe tip in water for the LD, MD, and HD surfaces measured at 26 °C (a) and 40 °C (b). The zero position of the tip is expediently defined as the starting position of the linear part in raw force data.

sharpness of these features, but there was no evidence for a dramatic structural change across the LCST. These observations suggest that the grafting density has a critical influence on the structural changes caused by increasing temperature in grafted PNIPAM layers. A sharp, discontinuous morphology change, due to mainly lateral aggregation of the grafted chains on these lower graft density surfaces, becomes a gradual continuous change that starts below the bulk solution LCST for higher graft densities. The AFM images suggest that the phase transition point becomes less definite with increasing grafting density.

We also measured the interaction forces between the AFM probe tip and the grafted PNIPAM surfaces. Typical force−distance profiles when the probe tip approaches the grafted PNIPAM before (26 °C) and after (40 °C) the observed phase transitions are given in parts a and b of Figure 2, respectively. The apparent separation distance between the surfaces was determined from the point of hard-wall contact deduced from the constant compliance region of the raw force data (force versus piezo-position curve).[47] It should be noted that zero distances determined here merely indicate the point of hard-wall contact where the grafted polymer layer no longer is compressed under the cantilever tip. Therefore, each surface is expected to have a different offset from the true bare surface zero distance to the apparent distance shown in the graph because the thickness of the polymer layer when it is fully compressed is presumed to be different for each surface.[48] Notwithstanding this issue, it is useful to observe the shape of the force−distance curves toward the point of apparent hard-wall contact and to highlight the qualitative differences between them depending on the grafting density.

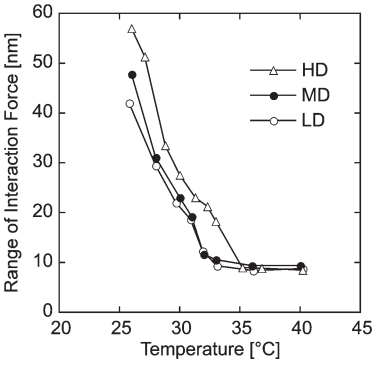

Figure 3. Change in the range of interaction forces between the PNIPAM layer and probe by temperature.

At 26 °C, the force curves indicate a monotonically increasing repulsion, presumably due to the large repulsive steric interaction between the bare tip and the grafted surface polymer chains. The repulsive force was seen to commence at apparent separation distances of approximately 40−60 nm for all three surface types. The semilog plot of the repulsive force for the HD surface gave an almost straight line across the whole distance of the measured interaction until the surfaces came into hard contact. In contrast to this, the profile of the force−distance data for the LD surface was initially less steep than that for the HD surface at large apparent distances. However, the forces were seen to increase dramatically as the surfaces came close, especially when the apparent distance was less than ca. 10 nm. The curve for the MD surface took somewhat intermediate values between the curves for the LD and HD surfaces. These force−distance profiles reflect qualitatively the features which are expected for different graft densities: for the HD surface, conformational degrees of freedom of the chains is severely restricted due to the high density, resulting in a strong resistance against the compression by the tip. On the other hand, the brush layer has much more lateral freedom for the LD surface, allowing the chains to partially collapse under the approaching probe tip and thereby reducing the resistance force at large apparent distances. Eventually, even in the LD case the polymer chains will lose this mobility due to compression by the tip, resulting in the observed increases in the repulsive force as a function of distance with decreasing separation.

A repulsive force was also seen for all the surface types at 40 °C, but the range of the force was significantly reduced. This is consistent with a collapse of the polymer chains at temperatures well above the LCST. Interestingly, the all the force data apparently have a similar form as a function of the distance, in contrast with the data obtained at 26 °C. While the chains are expected to be almost fully collapsed at this temperature, the measured repulsion indicates that the outer regions of the collapsed polymer layers are not completely stiff and some deformation of these layers by the probe tip must occur. The obtained force curves suggest that the degree of deformation in this state is almost identical and independent of the grafting density at this temperature; in other words, the mechanical properties of these layers are consistent under these conditions.

In Figure 3, we plot the apparent range of the repulsive interaction forces, estimated from the force curves, for each surface as a function of temperature. Again, it is worth noting that this plot merely shows the distance over which the polymer layer can be compressed by the tip. Uncertainty in the position of a true zero-distance for the force data in

terms of the underlying bare surfaces does not allow absolute distances to be determined. Nonetheless, we expect to obtain qualitative information about vertical structural changes of the chains, since the forces directly reflect the behavior of a grafted layer when compressed by a probe tip. As shown in Figure 3, the range over which the layer can be compressed reduces with increasing temperature, even well below the LCST, for all the surfaces. In contrast, the value becomes constant at higher temperatures, well above the LCST. These data indicate that for all the grafted layers, regardless of initial graft density, there is a significant collapse of the layer toward the surface over a broad range of temperature, particularly below the LCST. For the LD and MD surfaces, this tendency is quite different from the lateral structural change observed in the AFM images, which suggested a significant structural change within only a very narrow range of temperature close to the LCST. The data for the HD surface show collapse over a slightly broader temperature range than for the other surfaces. These data further suggest that the grafting density has an effect on the structural changes in the layer; this time we see the vertical collapse of these layers.

Values of Δf and ΔD for the PNIPAM-grafted QCM crystals at the three grafting densities and as a function of water temperature are shown in parts a and b of Figure 4, respectively. The inset of each figure shows a close-up graph of the plot for the LD and the MD surfaces. Each data point in the graph indicates the value when Δf and ΔD reach equilibrium at the given temperature. For each data set, the values obtained using an uncoated crystal, which changes linearly with temperature attributed to the variation of the viscosity and density of water with temperature, were subtracted as a background.

For the LD surface, Δf was seen to initially decrease slightly and then drop sharply around the temperature close to the LCST. After reaching a maximum negative value at 34 °C, Δf was then seen to increase steeply with further increases in temperature up to the maximum tested value of 40 °C. These changes of Δf against temperature are very similar to those we reported previously for a low-grafting density and high-molecular-weight surface.[41] Thus, we can apply the same analysis to the origins of the change in Δf as the previous results: upon dehydration and collapse toward phase transition, the chains will tend to couple more effectively to the motion of the oscillating sensor. This results in an increase in the "effective" mass registered on the surface which sets the Δf value negative. This effect must exceed the initial mass loss by dehydration of the chains and causes the net decrease of Δf. After the phase transition, a decrease in Δf caused by further conformation changes is relatively small, whereas the continued dehydration of the polymer chains and the densification of the layer resulting in the loss of physically coupled water from the layer results in a net increase in Δf.

This complex feature of the Δf data was significantly altered with increased grafting density. For the MD surface, Δf was seen to slowly increase with increasing temperature up to about 31 °C: It then decreased very slightly around the LCST. Above the LCST, Δf increased again very steeply up to 40 °C. For the HD surface, Δf showed only a large positive increment with increasing temperature. It is noteworthy, however, that the rate change in Δf is seen to decrease around the LCST. This behavior of Δf against grafting density is again interpreted in terms of the balance between changes in the coupling of the grafted polymer layer to the crystal and the loss of water from the PNIPAM layer, both by polymer dehydration and through changes in the "effective" mass due

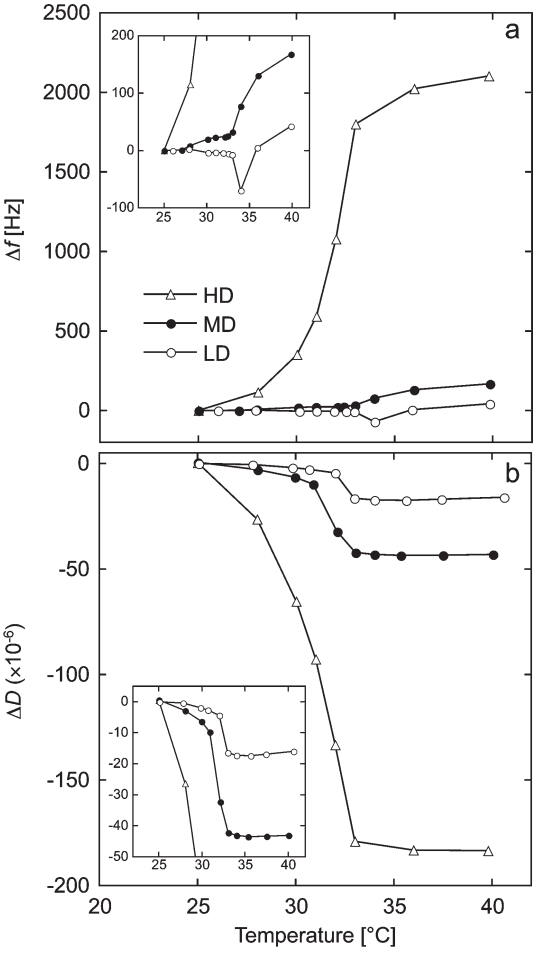

Figure 4. Changes in frequency, Δf (a), and dissipation, ΔD (b), depending on temperature for PNIPAM coated crystal in water for the LD, MD, and HD surfaces. The insets show the detailed behavior of the data for the LD and MD surfaces on enlarged scales. Each data point in the graph indicates the value when Δf and ΔD reach equilibrium at the given temperature where the value for a bare (uncoated) crystal are subtracted from each data point.

to the loss of water from within the layer due to the vertical collapse of the grafted polymer chains mentioned above. As the grafting density increases, the effect of an enhanced coupling of the grafted polymers as the temperature increases will be reduced since the polymer film is already expected to have significant mechanical integrity. This is supported by the AFM force−distance data as a function of the graft density (Figure 2). This reduced effect of changes in the polymer coupling signal mean that at higher graft density we expect the loss of water from the layer to be the dominant feature. Hence, the steady increase in the value of Δf which is observed and which is consistent with a loss of mass from the crystal.

Changes in the dissipation, ΔD, as a function of the temperature have a similar form for each of the surfaces tested here. For the LD surface the data show an initial slow decline in ΔD below the LCST. Then, at around the LCST, ΔD drops abruptly and discontinuously. After this, the value remains almost unchanged up to 40 °C. These data are in good agreement with our previous report.[41] The sudden drop in ΔD suggests, once again, a strong lateral aggregation of the PNIPAM chains at the LCST, leading to a collapsed and relatively compact surface polymer film consistent with the decrease in dissipation. Since a rigid layer has a lower energy dissipation compared to a flexible one,[49] the negative drop in

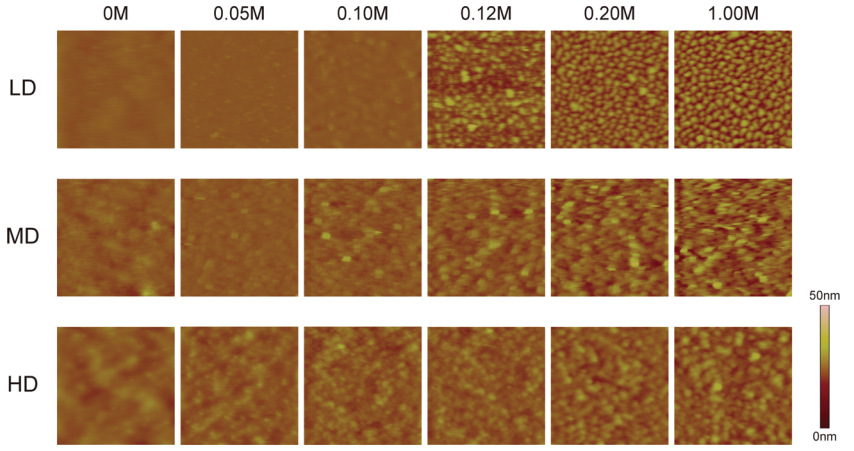

Figure 5. AFM images ($1 \times 1\ \mu m^2$) of a PNIPAM layer on silicon wafer in Na_2SO_4 solutions for the LD, MD, and HD surfaces at 26 °C. Images were obtained in 0, 0.05, 0.10 0.12, 0.20, and 1.00 M solutions.

the dissipation is seen. Changes in ΔD for the MD surface are the same as that for the LD surface: ΔD drops slowly from the room temperature value before also showing a relatively large drop in value near the LCST. Interestingly, the onset of this larger change in the dissipation is seen at a lower temperature than was observed for the LD surface, consistent with the observations from the AFM images. For the HD surface, ΔD was seen to constantly decline from well before the bulk solution LCST until just above it. This result also corresponds well to the observed behavior from the AFM images, which indicated that the phase transition of the grafted PNIPAM commenced well below LCST. These ΔD data strongly suggest that the lateral aggregation of the PNIPAM chains is the main contributor to the changes in ΔD.

In Salt Solution. We also conducted a similar set of experiments in Na_2SO_4 solutions at 26 °C. AFM images of the PNIPAM layer in Na_2SO_4 at various concentrations are shown in Figure 5. The LD surface again showed a sudden phase transition—in this case at a salt concentration of 0.12 M. The concentration at which the phase transition occurs for PNIPAM in Na_2SO_4 is the same as that found in our previous report.[42] Increasing graft density shows a similar influence on the phase transition as was seen for the temperature induced collapse data. For the MD surface polymer structures can already be seen at around 0.10 M, which is lower than the bulk solution phase transition concentration, and the phase transition seems to occur over a wider range of concentration. For the HD surface, only a very small increase of concentration seems to induce chain aggregation, as the domain structures are clear even at a concentration of 0.05 M. The phase transition is now continuous for this surface, as was the case for the temperature data.

The increase in Na_2SO_4 concentration also caused qualitatively similar changes in the values of Δf and ΔD from the QCM experiments, as shown in Figure 6. Δf was seen to have a clear negative peak at the concentration around 0.12 M. This negative peak is again attributable to the balance between structure-change effects and mass reduction caused by the water release from the surface. With increasing grafting density, for the MD surface, the negative peak of Δf decreases, and after the peak, Δf increases more steeply. For the HD surface, the negative peak disappeared completely, and Δf only showed increment as the concentration was increased. These behaviors are again attributable to the large mass loss due to the water desorption from dense chains exceeding structure-collapsing effect.

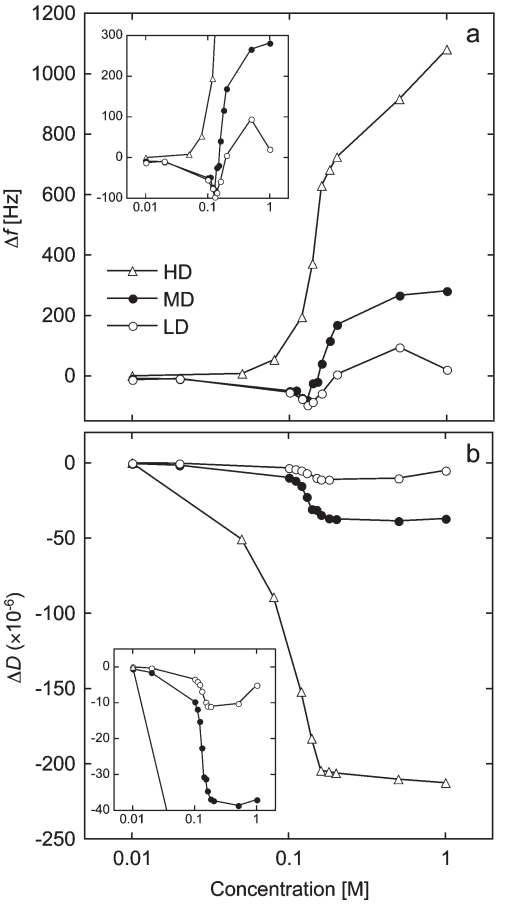

Figure 6. Changes in frequency, Δf (a), and dissipation, ΔD (b), depending on temperature for the PNIPAM-coated crystal in water for the LD, MD, and HD surfaces. The insets show the detailed behavior of the data for the LD and MD surfaces on enlarged scales. Each data point in the graph indicates the value when Δf and ΔD reach equilibrium at the given concentration where the values for a bare (uncoated) crystal are subtracted from each data point.

ΔD declined only slightly at dilute solutions and dropped abruptly and discontinuously at around 0.12 M. After this, ΔD was seen to increase, but its magnitude is not so large. This reflects that the PNIPAM layer becomes rigid by forming a collapsed mushroom-like state. ΔD dropped from room temperature to around the LCST, and after this, ΔD was seen to decrease very little with increasing temperature.

However, the drop before the LCST for the MD surface ΔD became steep and more continuous compared to that for the LD surface. For the HD surface, the change of ΔD before LCST was completely continuous. This result is again corresponding well to observation of the AFM images.

Chain Collapse and Phase Transition. The present study has shown that the structural transition of grafted PNIPAM in water when temperature is increased toward the LCST becomes more gradual with increasing grafting density. The experiments conducted in Na_2SO_4 solutions also showed the same tendency against grafting density on the phase transition when the salt concentration is increased. To the authors' knowledge, this is the first study to provide direct experimental evidence that the morphological structure of grafted PNIPAM chains strongly depends on grafting density of the chains.

The apparent range of the repulsive interaction forces (Figure 3) deduced from the steric repulsion forces between the probe tip and the PNIPAM layers implies that vertical collapse of the grafted chains, in the range of grafting densities explored here, occurs gradually over a broad temperature range in contrast to a sharp coil−globule transition observed for isolated polymer in bulk solution[50] or for grafted polymer with a high molecular weight and a low grafting density.[19,20] Of course, we could not estimate the exact layer thickness before and after phase transition, which is sometimes used as an indicator of the magnitude of the conformational change. Nonetheless, our force data at least indicate vertical collapse is taking place gradually over a wide range of temperatures even for the LD surface. Such a gradual vertical collapse is in accordance with results obtained from SPR,[22] NR,[23−27] QCM,[28−31] and SFA[37] measurements and our previous AFM result.[41] It is also qualitatively consistent with theoretical studies by Zhulina et al.,[40] which suggested that the collapse of a dense brush occurs gradually as the solvent condition became worse because of the repulsive interactions between stretched chains. On the other hand, grafting density does not have critical effect on the range of temperature over with the vertical collapse occurs. Although the range became a little broader with increasing in grafting density, the "sharpness" of the vertical structural change seems not to change significantly by grafting density in the present case.

In contrast, our AFM images and QCM-D data indicate that the variation of grafting density affects more dramatically the structural changes in the layer caused by lateral aggregation of the chains. The temperature at which this lateral aggregation commences, and causes noticeable changes in the layer, is influenced critically by the grafting density. This suggests that the grafting density has somewhat different effect on the lateral and vertical collapse for the grafted PNIPAM chains. The aggregation of PNIPAM chains is assumed to occur primarily by the formation of interchain hydrogen bonding between dehydrated amide groups and the hydrophobic interaction between the dehydrated chains.[51] On the other hand, the average distance between neighboring grafted chains obviously becomes less with increasing grafting density. This must result in an increased frequency of contacts between polymer segments driven by standard thermal Brownian fluctuations.[52] This increase in interchain interactions facilitates the lateral aggregation of these chains at lower temperatures.

How do we explain the observed broad temperature range over which lateral aggregation for the HD surface is seen? For the high-density brush, the stretched state of the chains necessarily causes a loss of conformational free energy when compared to chains that can adopt a more random conformation.[53] Collapse of the chains in this layer into a more polymer-rich surface layer will release some of this conformational restriction. In addition to this, it is not unreasonable to suppose that the PNIPAM chain segments at high graft density, and closer to the surface within the layer, are less hydrated. This, along with their more close-packed conditions, may facilitate interchain attractive interactions (H-bonding and/or hydrophobic). This too will facilitate lateral aggregation at a lower initial temperature. Clearly, the variation in polymer segment density away from the surface, for a dense brush layer,[54] suggests that there will be differences in the local environment between the outermost segments (effectively a low density domain) and those closer to the surface. These local variations in conditions clearly can have an effect on the aggregation of the layer, and this difference in local segment conditions through the layer may explain the wider temperature range seen for the response. At low graft density, all chains essentially behave as isolated coils, leading to much less of a difference between segments as we move away from the surface through the grafted layer.

It is also worth noting that the shape for the aggregates of the PNIPAM chains differs depending on the grafting density as seen in images both in water above LCST and in Na_2SO_4 above the phase transition concentration. The domain structures appeared on the LD surface seem relatively uniform, and the boundaries between them are very distinctive. On the other hand, increasing grafting density makes the structure less uniform with rather obscure, shallow boundaries. Particularly, the image of the aggregates on the HD surface seems irregular compared to the lower density surfaces. This tendency corresponds qualitatively to the results by theoretical investigations,[55−57] predicting that grafted chains forming well separated clusters at low grafting density at poor solvent condition, while these clusters are unstable at high grafting density. Yeung et al.[55] suggested that this effect would be caused by a large degree of the stretching of chains in the dense brush. Our AFM images provide clear experimental evidence that varying grafting density of polymer brush causes such changes in aggregate structure at poor solvent condition.

Conclusion

It is important to understand what affects the conformational changes of surface-grafted PNIPAM as a function of the graft density. In this paper, we focused on grafting density as a factor affecting on the phase transition. *In situ* AFM imaging showed that the conformational transition of a grafted PNIPAM layer from a brush-like to a mushroom-like state was clearly dependent on the grafting density: The image changes abruptly from featureless to showing localized domain structures at the LCST for a low density surface, whereas the change of structure was more gradual over a broader temperature range with increasing the grafting density. Frequency and dissipation data obtained using a QCM-D showed a significant change at the LCST for the low-density surface: the frequency had a negative peak, and dissipation dropped sharply at the LCST. With increasing grafting density, the negative peak decreased and the dissipation change became less steep. Similar effects were seen for the corresponding phase transition in sodium sulfate solutions as a function of increasing salt concentrations. These data confirmed that the PNIPAM structural transition depended strongly on the grafting density: increased graft density leads to less dramatic structural changes in the grafted polymer film, but these changes start at lower temperatures, below the LCST, and change in the layer continue over a broader range of temperatures.

As mentioned in the Introduction, the molecular weight, as well as the grafting density, has a critical importance on the structural behavior of PNIPAM brushes on surfaces. We are exploring the

influence of the molecular weight on the morphological behavior of end-grafted PNIPAM in current research and will report on this in future publications.

Acknowledgment. The authors acknowledge the financial support for this work from the Core-to-Core Program promoted by Japan Society for the Promotion of Science (Project No. 18004). N.I. is grateful to Dr. H. Kawasaki of Kansai University for helpful suggestions and comments.

References and Notes

(1) Heskins, M.; Guillet, J. E. *J. Macromol. Sci., Chem.* **1968**, *A2*, 1441–1455.
(2) Kanazawa, H.; Yamamoto, K.; Matsushima, Y.; Kikuchi, A.; Sakurai, Y.; Okano, T. *Anal. Chem.* **1996**, *68*, 100–105.
(3) Yakushiji, T.; Sakai, K.; Kikuchi, A.; Aoyagi, T.; Sakurai, Y.; Okano, T. *Anal. Chem.* **1999**, *71*, 1125–1130.
(4) Kobayashi, J.; Kikuchi, A.; Sakai, K.; Okano, T. *Anal. Chem.* **2001**, *73*, 2027–2033.
(5) Osada, Y.; Honda, H.; Ohta, M. *J. Membr. Sci.* **1986**, *27*, 327–338.
(6) Park, Y. S.; Ito, Y.; Imanishi, Y. *Langmuir* **1998**, *14*, 910–914.
(7) Chen, J. H.; Yoshida, M.; Maekawa, Y.; Tsubokawa, N. *Polymer* **2001**, *42*, 9361–9365.
(8) Yoshioka, H.; Mikami, M.; Nakai, T.; Mori, Y. *Polym. Adv. Technol.* **1994**, *6*, 418–420.
(9) Abu-Lail, N. I.; Kaholek, M.; LaMattina, B.; Clark, R. L.; Zauscher, S. *Sens. Actuators, B* **2006**, *114*, 371–378.
(10) Yamato, M.; Konno, C.; Utsumi, M.; Kikuchi, A.; Okano, T. *Biomaterials* **2002**, *23*, 561–567.
(11) Voit, B.; Schmaljohann, D.; Gramm, S.; Nitschke, M.; Werner, C. *Int. J. Mater. Res.* **2007**, *98*, 646–650.
(12) Okano, T.; Yamada, N.; Okuhara, M.; Sakai, H.; Sakurai, Y. *Biomaterials* **1995**, *16*, 297–303.
(13) Cunliffe, D.; Alarcon, C. D.; Peters, V.; Smith, J. R.; Alexander, C. *Langmuir* **2003**, *19*, 2888–2899.
(14) Okano, T.; Kikuchi, A.; Sakurai, Y.; Takei, Y.; Ogata, N. *J. Controlled Release* **1995**, *36*, 125–133.
(15) Akiyama, Y.; Kikuchi, A.; Yamato, M.; Okano, T. *Langmuir* **2004**, *20*, 5506–5511.
(16) Duracher, D.; Elaissari, A.; Mallet, F.; Pichot, C. *Langmuir* **2000**, *16*, 9002–9008.
(17) Taniguchi, T.; Duracher, D.; Delair, T.; Elaissari, A.; Pichot, C. *Colloids Surf., B* **2003**, *29*, 53–65.
(18) Ionov, L.; Stamm, M.; Diez, S. *Nano Lett.* **2006**, *9*, 1982–1987.
(19) Zhu, P. W.; Napper, D. H. *J. Chem. Phys.* **1997**, *106*, 6492–6498.
(20) Zhu, P. W.; Napper, D. H. *Colloids Surf., A* **1996**, *113*, 145–153.
(21) Walldal, C.; Wall, S. *Colloid Polym. Sci.* **2000**, *278*, 936–945.
(22) Balamurugan, S.; Mendez, S.; Balamurugan, S. S.; O'Brien, M. J., II; López, G. P. *Langmuir* **2003**, *19*, 2545–2549.
(23) Yim, H.; Kent, M. S.; Huber, D. L.; Satija, S.; Majewski, J.; Smith, G. S. *Macromolecules* **2003**, *36*, 5244–5251.
(24) Yim, H.; Kent, M. S.; Mendez, S.; Balamurugan, S. S.; Balamurugan, S.; Lopez, G. P.; Satija, S. *Macromolecules* **2004**, *37*, 1994–1997.
(25) Yim, H.; Kent, M. S.; Satija, S.; Mendez, S.; Balamurugan, S. S.; Balamurugan, S.; Lopez, C. P. *J. Polym. Sci., Part B* **2004**, *42*, 3302–3310.
(26) Yim, H.; Kent, M. S.; Mendez, S.; Lopez, G. P.; Satija, S.; Seo, Y. *Macromolecules* **2006**, *39*, 3420–3426.
(27) Yim, H.; Kent, M. S.; Satija, S.; Mendez, S.; Balamurugan, S. S.; Balamurugan, S.; Lopez, G. P. *Phys. Rev. E* **2005**, *72*, 051801.
(28) Zhang, G. *Macromolecules* **2004**, *37*, 6553–6557.
(29) Liu, G.; Zhang, G. *J. Phys. Chem. B* **2005**, *109*, 743–747.
(30) Liu, G.; Cheng, H.; Yan, L.; Zhang, G. *J. Phys. Chem. B* **2005**, *109*, 22603–22607.
(31) Annaka, M.; Yahiro, C.; Nagase, K.; Kikuchi, A.; Okano, T. *Polymer* **2007**, *48*, 5713–5720.
(32) Kidoaki, S.; Ohya, S.; Nakayama, Y.; Matsuda, T. *Langmuir* **2001**, *17*, 2402–2407.
(33) Ishida, N.; Kobayashi, K. *J. Colloid Interface Sci.* **2006**, *297*, 513–519.
(34) Jones, D. M.; Smith, J. R.; Huck, W. T. S.; Alexander, C. *Adv. Mater.* **2002**, *14*, 1130–1134.
(35) Plunkett, K. N.; Zhu, X.; Moore, J. S.; Leckband, D. *Langmuir* **2006**, *22*, 4259–4266.
(36) Zhu, X.; Yan, C.; Winnik, F. M.; Leckband, D. *Langmuir* **2007**, *23*, 162–169.
(37) Malham, I. B.; Bureau, L. *Langmuir* **2010**, *26*, 4762–4768.
(38) Zhulina, E. B.; Borisov, O. V.; Pryamitsyn, V. A.; Birshtein, T. M. *Macromolecules* **1991**, *24*, 140–149.
(39) Chakrabarti, A. *J. Chem. Phys.* **1994**, *100*, 631–635.
(40) Mendez, S.; Curro, J. G.; McCoy, J. D.; Lopez, G. P. *Macromolecules* **2005**, *38*, 174–181.
(41) Ishida, N.; Biggs, S. *Langmuir* **2007**, *23*, 11083–11088.
(42) Ishida, N.; Biggs, S. *Macromolecules* **2007**, *40*, 9045–9052.
(43) Kong, X.; Kawai, T.; Abe, J.; Iyoda, T. *Macromolecules* **2001**, *34*, 1837–1844.
(44) Manne, S.; Cleveland, J. P.; Gaub, H. E.; Stucky, G. D.; Hansma, P. K. *Langmuir* **1994**, *10*, 4409–4413.
(45) Sauerbrey, G. *Z. Phys.* **1959**, *155*, 206.
(46) Sakai, K.; Smith, E. G.; Webber, G. B.; Schatz, C.; Wanless, E. J.; Bütün, V.; Armes, S. P.; Biggs, S. *J. Phys. Chem. B* **2006**, *110*, 14744–14753.
(47) Ducker, W. A.; Senden, T. J.; Pashley, R. M. *Langmuir* **1992**, *8*, 1831–1836.
(48) Kelley, T. W.; Schorr, P. A.; Johnson, K. D.; Tirrell, M.; Frisbie, C. D. *Macromolecules* **1998**, *26*, 4297–4300.
(49) Höök, F.; Kasemo, B.; Nylander, T.; Fant, C.; Sott, K.; Elwing, H. *Anal. Chem.* **2001**, *73*, 5796–5804.
(50) Schild, H. G.; Tirrell, D. A. *J. Phys. Chem.* **1990**, *94*, 4352–4356.
(51) Maeda, Y.; Higuchi, T.; Ikeda, I. *Langmuir* **2000**, *16*, 7503–7509.
(52) Wang, X.; Qiu, X.; Wu, C. *Macromolecules* **1998**, *31*, 2972–2976.
(53) Milner, S. T. *Science* **1991**, *251*, 905–914.
(54) Fleer, G. J.; Cohen Stuart, M. A.; Scheutjens, J. M. H. M.; Cosgrove, T.; Vincent, B. *Polymers at Interfaces*; Chapman & Hall: London, 1993.
(55) Yeung, C.; Balazs, A. C.; Jasnow, D. *Macromolecules* **1993**, *26*, 1914–1921.
(56) Grest, G. S.; Murat, M. *Macromolecules* **1993**, *26*, 3108–3117.
(57) Weinhold, J. D.; Kumar, S. K. *J. Chem. Phys.* **1994**, *101*, 4312–4323.